2018 IEEE-RAS 18th International Conference on Humanoid Robots (Humanoids)
Beijing, China, November 6-9, 2018

Semi-Passive Walk and Active Walk by One Bipedal Robot

Shintaro Noda, Fumihito Sugai, Kunio Kojima, Kim-Ngoc-Khanh Nguyen,
Yohei Kakiuchi, Kei Okada and Masayuki Inaba

***Abstract*— We developed a robot which can do both of active walking (all joints are actively controlled by actuators) and semi-passive walking (hip joints are passive and spring attached). In this paper, we summarize three technologies to achieve the development. The first one is small and high-strength clutch mechanism to sustain massive weight of life-size robot. The second one is semi-passive walk controller to consider passive joint dynamics. The last one is model parameter identification considering not only body parameters but also environment ones such as ground slope to achieve unstable motion similar to simulated result in real world.**

I. Background and Motivation

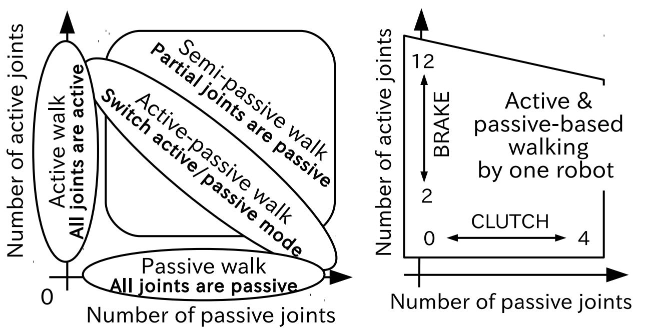

(a) Previous works were separated (b) Our target is to cover all

Fig. 1. Researches on active walking and passive-based walking were separated as shown in (a). Our target is to develop a robot to do all of active walking and passive-based walking as shown in (b).

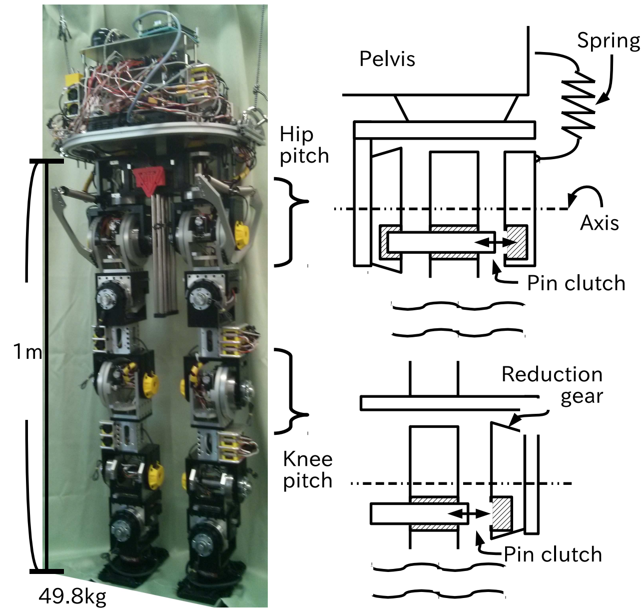

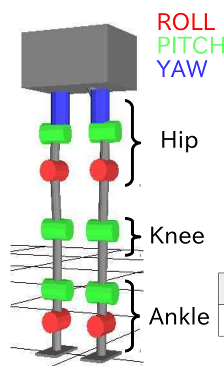

Joint Name	Clutch	Brake
Hip Yaw	-	-
Hip Pitch	yes	yes
Hip Roll	-	yes
Knee Pitch	yes	yes
Ankle Pitch	-	yes
Ankle Roll	-	yes

Gear Ratio	Max Torque	Range of Motion
160	220 Nm	[-1.57, 1.57] rad*

* Left image is all 0 radian joint angles

Fig. 2. Bipedal robot which has clutch mechanisms on hip pitch and knee pitch joints of both legs to do both of active walking and semi-passive walking. Hip has 3 joints, knee has 1 and ankle has 2 joints. Clutch mechanism is equipped with hip pitch and knee pitch joints. Gear ratio is 160, maximum joint torque is 220 [Nm] which is determined by ratcheting torque of harmonic gear and current limit of motor driver, and range of motion is from -1.57 [rad] to $+1.57$ [rad] for all joints.

Recently, robotics researchers have made great progress in development of bipedal robots; DURUS [1] has achieved energy-efficient walking, MARLO [2] has demonstrated robust push-recovery control, and the other robots such as [3][4][5][6][7][8][9][10][11] have also achieved unique applications in a few decades. However, these recent robots use mostly active joints. Walking with passive joints is known as passive walking [12] to distinguish from active walking in which all joints are actively controlled as [13]. If partial joints are passive and the others are active, such walking is sometimes called as semi-passive walking [14][15] to distinguish from pure passive walking in which all joints are passive as [12][16][15]. However, these bipedal robots with always-passive joints are limited to some particular uses. In many cases, the use is limited to passive walking and the other applications such as active walking are impossible.

The authors are with Graduate School of Information Science and Technology, The University of Tokyo, 7-3-1 Hongo, Bunkyo-ku, Tokyo 113-8656, Japan (s-noda at jsk.t.u-tokyo.ac.jp). This work was partially supported by Grant-in-Aid for JSPS Fellows (#15J08714).

A compromise idea of active walking and passive walking is active-passive walking with clutch-like mechanisms to switch active and passive mode of joints while walking. [17] proposes a mechanism using ball screw to switch active/passive mode of knee and ankle joints while walking. [18] proposes a backlash clutch mechanism, which is a simple and sophisticated idea for active/passive switching of knee joint while walking by using backlash. However, these mechanisms could exert joint torque only one direction in active mode, which makes position control difficult because

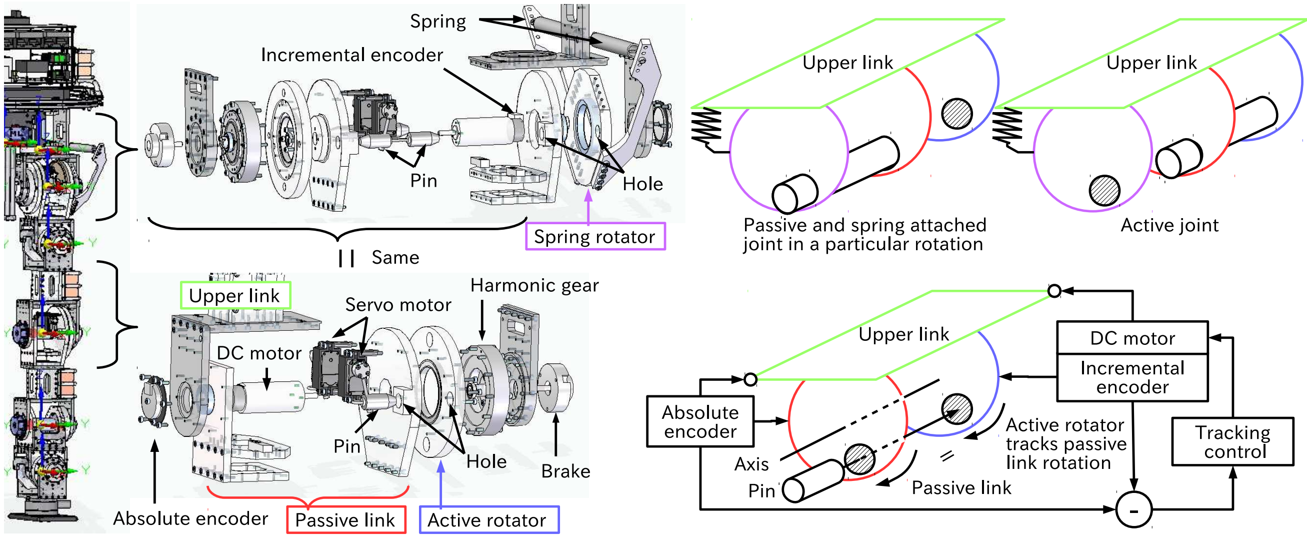

Fig. 3. Exploded views and schematic diagrams of clutch mechanisms on left knee and left hip joints are shown. Left exploded views show three independently rotators: passive link, active rotator and spring rotator. Spring rotator is embedded only on hip clutch. These three components are connected and disconnected by a pin driven by servo motor. To freely move the pin, active rotator is controlled to track passive link by tracking controller shown in bottom of right schematic diagram. The tracking controller cancels relative rotation between active rotator and passive link by using two encoders: absolute encoder to measure relative rotation between upper link and passive link, and incremental encoder to measure relative rotation between upper link and active rotator. Hip clutch has spring rotator to support upper body in passive joint mode. If pin is disconnected from active rotator, pin is connected to spring rotator and vice versa.

simple PD controller is unusable. Therefore, the applications were limited to active-passive walking.

In this way, previous researches on active walking and passive-based walking were separated as shown in Fig. 1. All robots which can do active walking can not do passive-based walking, and vice versa. Our motivation is to develop a robot which can do not only active motion but also passive-based motion to obtain both merits of highly-controllable active joint and energy-efficient passive joints. Actually, our robot shown in Fig. 2 has achieved both of active walking and semi-passive walking by one body. Further, active-passive walking will be possible although only active walking and semi-passive walking are shown in this paper. In this paper, we summarize the technologies to develop the robot. In section II, hardwares are described. We use dog clutch mechanism to switch active joint and passive joint of hip pitch and knee pitch joints of both legs. To create frictionless passive joint, clutch mechanism should be placed before gear reduction because large gear ratio causes large friction force. However, such clutch without reduction must transmit large joint torque to sustain massive body of life-sized robot. Further, spring mechanism to support upper body for passive walking is also described in the section. In section III, walking controllers are described. To consider passive joint dynamics, we use evolutionary search in dynamics simulator. To accelerate the search, we developed full-scratch dynamics simulator and parallelized the search algorithm. The performance is also described in the section. In section IV, walking experiments and model parameter identification of body and environment models are described. To achieve unstable semi-passive walking in real world, model parameter identification was indispensable. We use evolutionary search in dynamics simulator to detect a model parameter for the simulator to output similar result to real world experiment.

II. Design of Clutch and Spring Embedded on Leg

Our approach to switch active joint and passive joint by one leg is to use clutch mechanisms [19] which can control joint torque transmission. Because our robot is equipped with harmonic gears, small clutch mechanisms to transmit small torque is enough if the clutches are placed after gear reduction. However, high gear ratio causes high friction force and is not suitable for passive walking. If clutch mechanisms are placed before gear reduction, gear friction is cut off. However, the clutch mechanisms must transmit large joint torque. For example, life-sized humanoid robot JAXON [6] can exert over 300 Nm joint torque. A electromagnetic tooth clutch product [20] occupies 134 mm diameter times 83 mm height volume and consumes 56.6 W energy. Such friction clutch which transmits torque by friction between two faces becomes large because large area of friction face or large inner force between the faces are necessary to transmit large torque. In comparison with friction clutch, dog clutch which transmits torque by interference of two rotators becomes small. However, to switch active and passive mode by dog clutch, relative rotation between the rotators must be controlled to zero. We use actuator placed on each joint not only to rotate the joint but also to control the clutch rotators. The designs are shown in Fig. 3. Small pins are horizontally moved by small servo motors. If the pin is placed between two rotators, interference between pin and rotators transmit torque. In contrast, if the pin is placed on only one rotator, two rotators become independent. Fig.

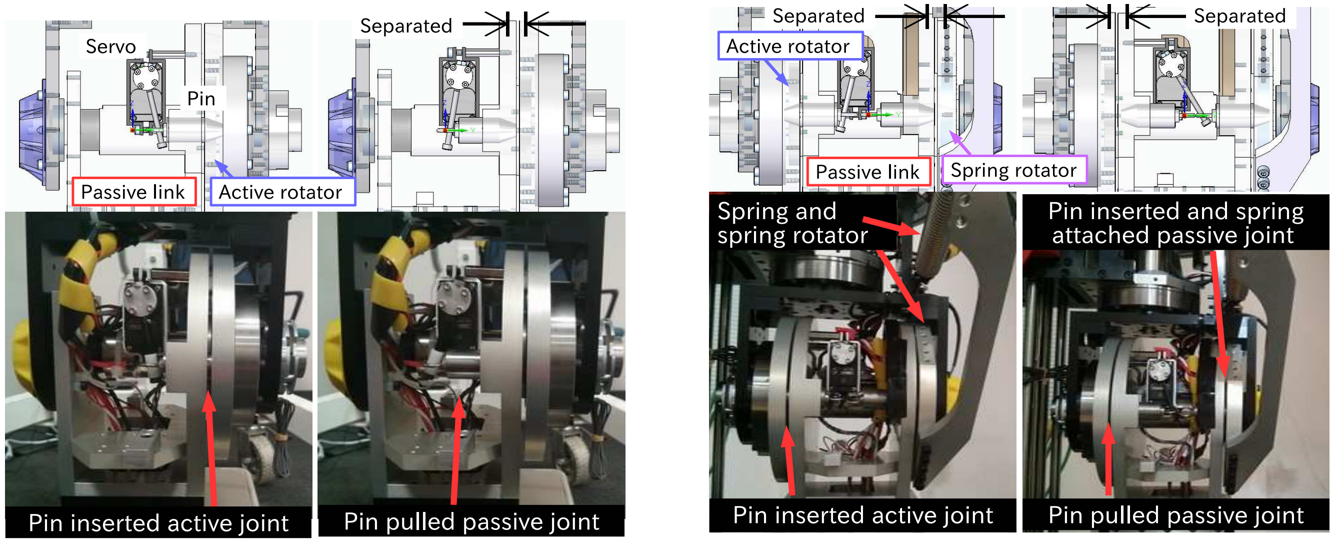

(a) Knee joint's active/passive mode

(b) Hip joint's active/passive mode

Fig. 4. Enlarged views of knee and hip clutch mechanisms including actual joints and CAD models. Left sides show active mode and pin is inserted, and right sides show passive mode and pin is pulled.

4 shows active and passive mode of (a) knee and (b) hip clutches. We can confirm that pin is placed in both of passive link and active rotator in active mode of both clutches. In passive mode, pin of knee clutch shown in Fig. 4.(a) is placed only in passive link. In contrast, pin of hip clutch in passive mode shown in Fig. 4.(b) is placed in both of passive link and spring rotator. The diameter of pin is determined for yield stress to be 10 times larger than the maximum stress when maximum joint torque are applied. The maximum joint torque is 220 Nm which is calculated from electric current limit and ratcheting torque of harmonic gear. Similar motor driver we used is described in [21]. DC motor placed on joint can rotate active rotator shown in Fig. 3. The motor rotates passive link by rotating active rotator when clutch pins are placed between passive link and active rotator. When the pins are placed only on passive link, the motor rotates only active rotator. Therefore, active rotator can track passive link in passive joint mode. There additionally exists spring rotator in hip pitch joint. The spring rotator connects body link and leg links by spring when pins are placed between passive link and spring rotator. The spring is necessary for passive walking with upper body [22]. [22] shows that there exists stable limit cycle for passive walking if upper body is always placed in the middle of both legs. However, such bisection mechanism disturb active motion. In our design, clutch mechanism disconnects spring rotator in active walking, and connects spring only in semi-passive walking.

III. Walk controller to consider passive joint dynamics and energy efficiency

To generate walking motion considering passive joint motion, planning algorithm involving forward dynamics is needed. In this paper, we determine controller model parameter for semi-passive walking by using evolutionary algorithm in dynamics simulator world. We use Featherstone's algorithm [23] for forward dynamics, and penalty method [24] to calculate contact force. The pseudo code is described in [25]. The implementation is by C++ language, the calculation speed is 70 kHz for 12-dof bipedal robot using Intel(R) Core(TM) i7-4770SCPU 3.10GHz. The evolutionary algorithm consists of mutation and amoeba method [26] and is implemented in non-linear optimization library NLopt [27]. Further, we additionally make a change to enable parallel computation. We use SIMBICON [28] as the controller model. SIMBICON is a finite state machine in which the state transits by contact change and spent time. Each state has target joint angle, and the states transition includes linear interpolation between the target joint angles and feedback controlling using position and velocity of CoG (Center of Gravity) of robot. The evolutionary algorithm searches the target joint angles and feedback gains. A paper about the walk controller will appear in IROS 2018 [29]. In this paper, objective of walking controller search is CoT, which is energy consumption per unit mass and unit CoG velocity. CoT in simulation world is calculated according to the following equations:

$$
\begin{aligned}
CoT &= \frac{E}{mgd} \qquad (1)\\
E &= \sum\nolimits_{i\in[0,N)} \left(\dot{E}_i^k + \dot{E}_i^t + \dot{E}_i^c\right)\Delta t\\
s.t. &\left\{\begin{array}{lcl} \dot{E}_i^k & = & \boldsymbol{\tau}_i^T \boldsymbol{\omega}_i \\ \dot{E}_i^t & = & R\boldsymbol{I}_i^T\boldsymbol{I}_i \\ \dot{E}_i^c & = & Constant \end{array}\right.
\end{aligned}
$$

We consider kinetic energy $\dot{E}_i^k$ at i-th simulation time step, thermal loss $\dot{E}_i^t$ and other energy consumption $\dot{E}_i^c$ including CPU power source. The kinetic energy $\dot{E}_i^k$ is calculated by using joint torque $\boldsymbol{\tau}_i$ and joint angular velocity $\boldsymbol{\omega}_i$ which are

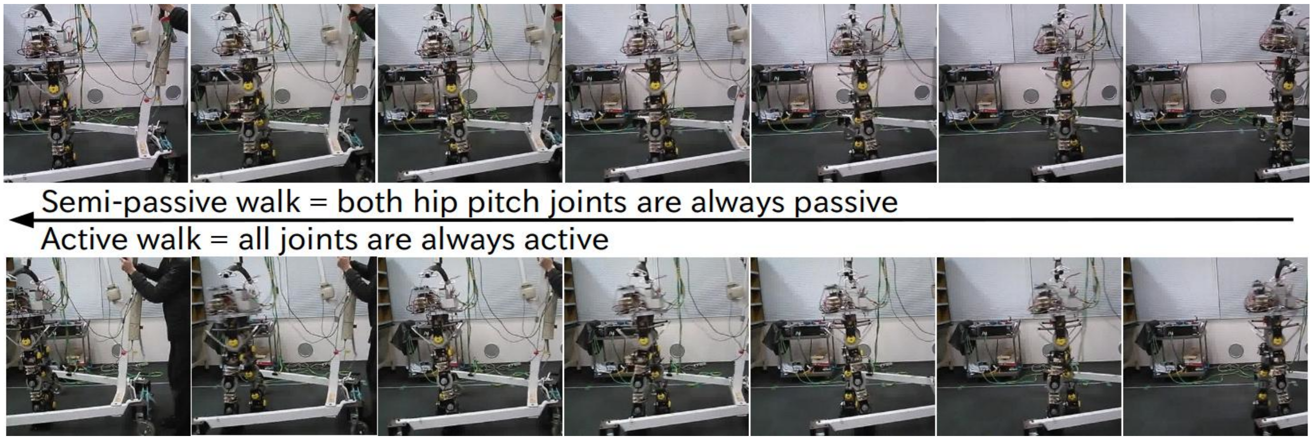

Fig. 5. Snapshots of semi-passive walking and active walking experiment. Semi-passive means both hip pitch joints are always passive and the other joints are active.

easily obtained in forward dynamics calculation. The thermal loss is calculated by using constant electric resistance R and electric current $\boldsymbol{I}_i$ which is obtained from $\boldsymbol{I}_i = A_r^{-1}\boldsymbol{\tau}$ (A_r^{-1} = Torque Constant). $\dot{E}_i^c$ is average energy consumption of actual robot with zero joint torque. m is total mass of robot, g is gravity constant and d is movement distance of walking.

Constraints of search are as follows:

- Maximum joint torque is 80 Nm
- Maximum joint velocity is 1.5 rad/s
- Maximum contact moment is 50 Nm
- Self collision and environment collision excluding foot
- Minimum height of pelvis link above ground is 80 cm
- Maximum simulation time t_m is 10 s (Success condition)

The search process changes controller parameter, simulates, calculate the first time when the constraints are not satisfied, and calculate the following objective:

$$Minimize \begin{cases} 1/(1+\frac{1}{CoT}) & (t \geq t_m) \\ t_m/t & (t < t_m) \end{cases} \quad (2)$$

If the success condition is not satisfied ($t < t_m$), the objective becomes proportion to time duration in which constraints are satisfied to detect parameter for walk without falling. If the success condition is satisfied ($t \geq t_m$), the objective becomes to include CoT to detect energy efficient parameter. The reason why we did not directly use CoT as objective is that falling motion sometimes becomes small CoT motion if robot vigorously falls forward and such motion can become local optima. The objective aims at searching only not-falling walk motion.

Fig. 6 shows transitions of objective and CoT while searching. The search uses two conditions: active walking (act) using all joints as active, and semi-passive walking (pas) using hip pitch joints of both legs as passive. The search uses 7 thread parallel computation and detect 10 seconds walking motions without initial guess. Right axis shows objective (Eq. 2). If the objective is less than 1, walking motion is stable in 10 seconds. We can confirm that 0.05 days searching detects both of active walking and semi-passive walking parameters. After 0.8 days searching, CoT becomes about 2.5 for semi-passive walking and 3.2 for active walking. There are two reasons why the CoT is a few times larger than previous research [1]. First reason is that our walking simulation includes starting and stopping of walk motion. Forward movement is small in starting and stopping motions. Further, the movement is zero after stopping. Although our walk controller stops robot around 6 seconds, simulation continues 10 seconds to check that robot does not fall. Actually, we confirmed that CoT decreased to 1.41 if we simulated 100 seconds walking motion using the same semi-passive walking parameter. Second reason is that our robot uses small gear ratio (160) and large electric current loses lots of energy. We confirmed that walking motion was possible with 500 gear ratio and CoT decreased to 0.9 in simulation.

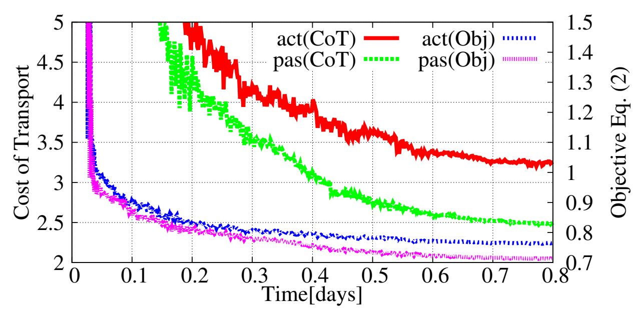

Fig. 6. Transitions of objective and CoT while searching active walking (act) and semi-passive walking (pas)

IV. Walk experiments by model identification and motion regeneration Loop

In section III, we detected walking controller in simulation world. However, the parameter was not stable in real world. Although one point of view of this failure is that walking controller is not stable enough, essentially, the failure derive from difference of body and environment model parameter between real world and simulation world. If the model parameters are accurate, walking is possible without stabilizing control. There exist two important previous researches about model identification. [30] minimizes error of sensor outputs between real world and simulation world and identifies center of gravity position of each link. [31] proposes an identification method of dynamics parameters using equation of motion. Although [30] needs lots of computational time, the approach can identify all parameters in simulation including friction and ground slope. Further, the approach is easy to use with our walking controller searched in simulation world. Therefore, we use [30] approach. We use following model error as objective of model identification:

$$Minimize\sqrt{\frac{||\boldsymbol{q}-\boldsymbol{q}'||^2+||\boldsymbol{p}-\boldsymbol{p}'||^2+||\boldsymbol{r}-\boldsymbol{r}'||^2}{M(2N+3)}} \tag{3}$$

$\boldsymbol{q}$ is all joint angles measured by rotational encoder in 100 Hz. $\boldsymbol{p}$ is all target joint angles. $\boldsymbol{r}$ is estimated value of root link attitude. For the estimation of root link attitude, we use [32] method by using acceleration sensor and gyro sensor placed on pelvis link. $\boldsymbol{q}', \boldsymbol{p}', \boldsymbol{r}'$ are simulated value of $\boldsymbol{q}, \boldsymbol{p}, \boldsymbol{r}$. N is total number of joints of robot. M is total number of sampling of sensor values. $\boldsymbol{r}'$ which is simulated root link attitude is calculated by using the same algorithm [32] as real world $\boldsymbol{r}$. Because our walking controller described in section III includes feedback term, target joint angles $\boldsymbol{p}$ is generally different from simulated value $\boldsymbol{q}'$. By using both of target joint angles $\boldsymbol{p}$ and measured angles $\boldsymbol{q}$, joint torque affects the model identification because we use PD controller for position control of robot and distance between target joint angles and measured values determines electric current input to actuator. Search parameters are shown in TABLE I-II. The parameters include dynamics parameters of links and contact parameters such as friction coefficient.

TABLE I

JOINT MODEL AND LINK MODEL PARAMETER

Description	Range	Dim
Total weight of link	±1 kg	1
Center of gravity in local frame	±0.1 m	3
Inertia Tensor around center of gravity	±0.01 kgm^2	6
Relative position between parent joint	±0.001 m	3
Relative attitude between parameter joint	±0.1 deg	3
PD gain of position controller	±10 %	2
Rotary encoder offset	±0.5 deg	1
Total		19N

TABLE II

CONTACT MODEL AND SENSOR MODEL PARAMETER

Description	Range	Dim
Threshold of contact change	±15 N	1
PD gain to calculate contact force	±10 %	2
PD gain to calculate friction force	±10 %	2
Friction coefficient of contact	±0.4	1
Friction coefficient of passive joint	±0.005	1
Spring constant	±300 N/m	1
Acceleration sensor and gyro sensor offset	±0.5 deg	3
Slope of ground	±0.5 deg	2
Foot vertices for contact (8 points)	±0.005 m	24
Total		37

Search process changes the parameters and simulates to minimize the model error (Eq. 3). Initial guess of link model parameters are determined from CAD value, and initial guess of contact model parameters are heuristically determined by checking simulation result of standing posture. Search algorithm is evolutionary one described in section III. We achieved active walking and semi-passive walking by repeating model identification described in this section IV and walk controller regeneration described in III. Results are show in Fig. 7 for active walking and Fig. 8 for semi-passive walking.

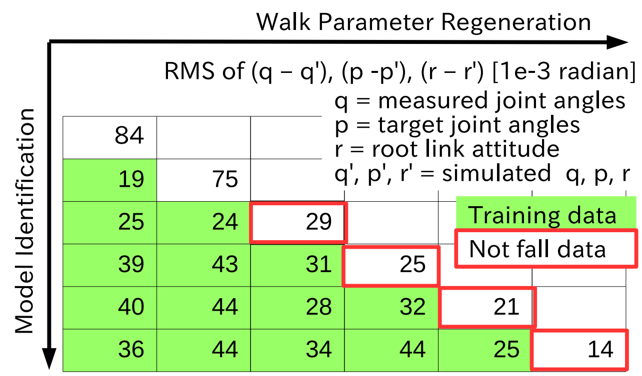

Fig. 7. Errors of model identification about active walking experiment

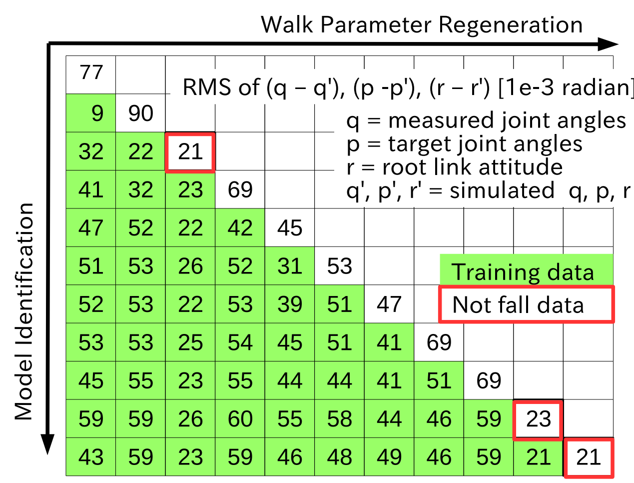

Fig. 8. Errors of model identification about semi-passive walking experiment

Model identification took 10 hours by using 7 parallel computation. Walk controller regeneration was also 10 hours and 7 parallel computation by using previous walk controller as initial guess. Each number in the figures shows error of model identification described as Eq. 3. The unit is 10^{-3} [radian]. Row of the figure separates model identification, column separates regenerated walk controller. After each model identification, new walk controller is generated. Therefore, the figures look like lower triangular matrix. Top row shows result without model identification and there is one walk controller only. Second row from top shows 2 numbers. Left-end column is used as training data for model identification and is highlighted in green. The number (Eq. 3) is smaller than top row. Third row from top shows 3 numbers. Left-end column and second left-end column are used as

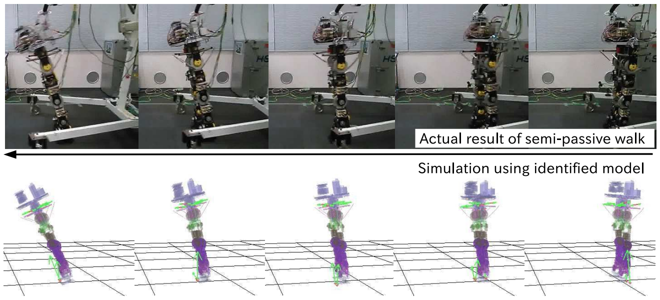

(a) Snapshot of semi-passive walking using the first walk controller.

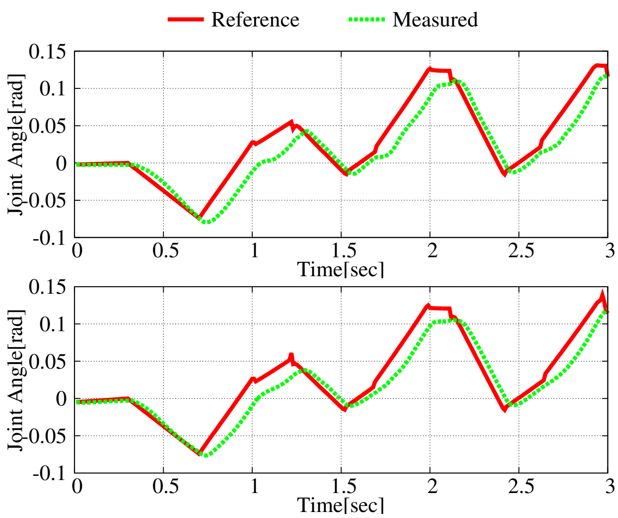

(b) Reference and measured hip roll joint angles.

Fig. 9. A result of model identification is shown. (a) Snapshot of walking experiments, and (b) Hip roll joint angles reference and target. Upper side of each figure shows actual result, and lower side shows simulated result after model identification.

training data. In Fig. 7, number at third column and third row is highlighted in red because our robot did not fall by using the controller. After third row, walking experiment succeeds by using regenerated walk controller. We can confirm that the model error decreases in every model identification. We had several similar experiments on active walking in addition to the experiment shown in this paper, and we obtained similar results. Fig. 8 shows result of semi-passive walking. 10 times model identification is needed to detect 3 not-fall walking controllers because semi-passive walking is unstable.

The identified model parameters are effective to simulate similar results for a particular motion used as training data. However, we assume that the parameters are not correct for all motions. Actually, we confirmed that the identified parameters of active walking and semi-passive walking were largely different. By using the identified parameter at 5-th row of active walking, we simulated the 10-th column semi-passive walk controller. The model error (Eq. 3) was 259×10^{-3} [radian]. It will be an important future work to check whether or not the difference disappear if we have more experiments.

Fig. 9 shows a partial result of model identification to compare actual result and simulated result. Walk controller is the first one of semi-passive walking (first column of Fig. 8). Fig. 9. (a) shows snapshot of walking experiment in real world (Upper side) and in simulation world (Lower side). Fig. 9. (b) shows reference and target hip roll joint angles. The joint had the largest joint torque while walking. Actual result and simulated result looks very similar.

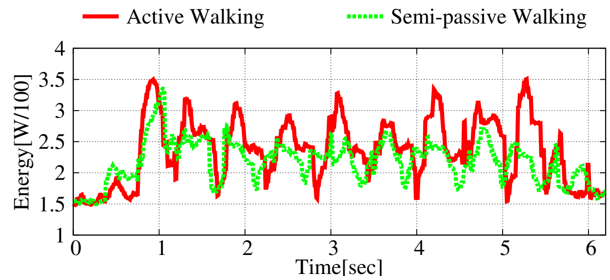

Fig. 10. Energy consumption of the last active walking (red) and semi-passive walking (green).

Fig.10 shows energy consumption of 5-th active walking and 10-th semi-passive walking in 6 seconds. Sum of energy is 1428.75 [J] for active walking and 1312.23 [J] for semi-passive walking. Because both hip pitch joints are always passive and the joints consume no energy while semi-passive walking, energy consumption of semi-passive walking is smaller than that of active walking. However, CoT of semi-passive walking is larger. Active walking moves 1.4 m and CoT is $1428.75/(49.8kg \times 9.8m/s^2 \times 1.4m) = 2.09$. Semi-passive walking moves 1.2 m and CoT is $1312.23/(49.8kg \times 9.8m/s^2 \times 1.2m) = 2.24$. Because simulated move distance is 1.5 m, we believe more accurate model identification is possible to reduce CoT.

V. Summary and Conclusion

We aimed at developing a robot which can do both of active walking and semi-passive walking, and solved three problems. First problem was design of leg equipped with pin-clutch mechanism and spring. Although dog clutch is a well-known mechanism, it is our contribution to show a practical solution for low friction passive joint in compact leg design. Second problem was walk controller to consider passive joint dynamics. We confirmed that evolutionary search of SIMBICON controller parameters in dynamic simulator was effective for the problem. Third problem was model identification to achieve simulated motion in real world. We identified not only dynamics parameter such as link weight but also contact model parameter such as friction and slope of ground. We assume that the effectiveness of our model identification was strongly evaluated by achieving unstable semi-passive walking in real world. This paper shows the first achievement to develop a robot which can do both of active walking and passive-based walking by one bipedal body. The achievement makes passive-based walking technology applicable to active-joint robots and has large effect on future robot development.

A. Future works

In addition to active walking and semi-passive walking shown in this paper, our robot can do two other types of walking; One is active-passive walking. Because knee joints of our robot are equipped with clutch mechanisms, knee joints could be switched between passive mode during swing phase and active mode during stance phase. The other is more underactuated walking by using brake. We assume that not only underactuated active walking but also underactuated semi-passive walking will be possible by our walk controller. Actually, semi-passive walking shown in this paper uses only 10 (less than 12) active joints for both legs.

REFERENCES

[1] A. Hereid, E. A Cousineau, C. M. Hubicki, and A. D. Ames. 3d dynamic walking with underactuated humanoid robots: A direct collocation framework for optimizing hybrid zero dynamics. In *IEEE International Conference on Robotics and Automation (ICRA)*, 2016.

[2] B. G. Buss, A. Ramezani, K. Akbari Hamed, B. A. Griffin, K. S. Galloway, and J. W. Grizzle. Preliminary walking experiments with underactuated 3d bipedal robot marlo. In *IEEE/RSJ International Conference on Intelligent Robots and Systems (IROS)*, pp. 2529–2536, Sept 2014.

[3] Y. Sakagami, R. Watanabe, C. Aoyama, S. Matsunaga, N. Higaki, and K. Fujimura. The intelligent asimo: System overview and integration. In *IEEE/RSJ International Conference on Intelligent Robots and Systems (IROS)*, Vol. 3, pp. 2478–2483, 2002.

[4] G. Nelson, A. Saunders, N. Neville, B. Swilling, J. Bondaryk, D. Billings, C. Lee, R. Playter, and M. Raibert. Petman: A humanoid robot for testing chemical protective clothing. *Journal of Robotics Society of Japan (JRSJ)*, Vol. 30, No. 4, pp. 372–377, 2012.

[5] Z. Li, N. G. Tsagarakis, and D. G. Caldwell. Walking pattern generation for a humanoid robot with compliant joints. *Autonomous Robots*, Vol. 35, No. 1, pp. 1–14, 2013.

[6] K. Kojima, T. Karasawa, T. Kozuki, E. Kuroiwa, S. Yukizaki, S. Iwaishi, T. Ishikawa, R. Koyama, S. Noda, F. Sugai, S. Nozawa, Y. Kakiuchi, K. Okada, and M. Inaba. Development of life-sized high-power humanoid robot jaxon for real-world use. In *IEEE-RAS International Conference on Humanoid Robots (Humanoids)*, pp. 838–843, Nov 2015.

[7] A. Stentz, H. Herman, A. Kelly, E. Meyhofer, G. C. Haynes, D. Stager, B. Zajac, J. A. Bagnell, J. Brindza, C. Dellin, M. George, J. Gonzalez-Mora, S. Hyde, M. Jones, M. Laverne, M. Likhachev, L. Lister, M. Powers, O. Ramos, J. Ray, D. Rice, J. Scheifflee, R. Sidki, S. Srinivasa, K. Strabala, J.P. Tardif, J. S. Valois, M. V. Weghe, M. Wagner, and C. Wellington. Chimp, the cmu highly intelligent mobile platform. *Journal of Field Robotics (JFR)*, Vol. 32, No. 2, pp. 209–228, 2015.

[8] N. G. Tsagarakis, D. G. Caldwell, F. Negrello, W. Choi, L. Baccelliere, V.G. Loc, J. Noorden, L. Muratore, A. Margan, A. Cardellino, L. Natale, E. Mingo Hoffman, H. Dallali, N. Kashiri, J. Malzahn, J. Lee, P. Kryczka, D. Kanoulas, M. Garabini, M. Catalano, M. Ferrati, V. Varricchio, L. Pallottino, C. Pavan, A. Bicchi, A. Settimi, A. Rocchi, and A. Ajoudani. Walk-man: A high-performance humanoid platform for realistic environments. *Journal of Field Robotics (JFR)*, Vol. 34, No. 7, pp. 1225–1259, 2017.

[9] O. Stasse, T. Flayols, R. Budhiraja, K. Giraud-Esclasse, J. Carpentier, J. Mirabel, A. Del Prete, P. Souères, N. Mansard, F. Lamiraux, J. P. Laumond, L. Marchionni, H. Tome, and F. Ferro. Talos: A new humanoid research platform targeted for industrial applications. In *IEEE-RAS International Conference on Humanoid Robots (Humanoids)*, pp. 689–696, Nov 2017.

[10] B. Henze, A. Dietrich, and C. Ott. An approach to combine balancing with hierarchical whole-body control for legged humanoid robots. *IEEE Robotics and Automation Letters (RAL)*, Vol. 1, No. 2, pp. 700–707, July 2016.

[11] T. Jung, J. Lim, H. Bae, K. K. Lee, H. M. Joe, and J. H. Oh. Development of the humanoid disaster response platform drc-hubo+. *IEEE Transactions on Robotics (TRO)*, Vol. 34, No. 1, pp. 1–17, Feb 2018.

[12] T. McGeer. Passive dynamic walking. *The International Journal of Robotics Research (IJRR)*, Vol. 9, No. 2, pp. 62–82, 1990.

[13] S. Kajita, F. Kanehiro, K. Kaneko, K. Fujiwara, K. Harada, K. Yokoi, and H. Hirukawa. Biped walking pattern generation by using preview control of zero-moment point. In *IEEE International Conference on Robotics and Automation (ICRA)*, pp. 1620–1626, Sept 2003.

[14] M. Wisse, G. Keliksdal, J. van Frankenhyyzen, and B. Moyer. Passive-based walking robot. *IEEE Robotics & Automation Magazine (RAM)*, Vol. 14, No. 2, pp. 52–62, 2007.

[15] Q. Li, G. Liu, J. Tang, and J. Zhang. A simple 2d straight-leg passive dynamic walking model without foot-scuffing problem. In *IEEE/RSJ International Conference on Intelligent Robots and Systems (IROS)*, pp. 5155–5161, Oct 2016.

[16] S. H. Collins, M. Wisse, and A. Ruina. A three-dimensional passive-dynamic walking robot with two legs and knees. *The International Journal of Robotics Research (IJRR)*, Vol. 20, No. 7, pp. 607–615, 2001.

[17] K. Koganezawa and O. Matsumoto. Active/passive hybrid walking by the biped robot tokai robo-habilis 1. In *IEEE/RSJ International Conference on Intelligent Robots and Systems (IROS)*, Vol. 3, pp. 2461–2466 vol.3, 2002.

[18] M. Okada, T. Shinohara, T. Gotoh, S. Ban, and Y. Nakamura. Double spherical joint and backlash clutch for lower limbs of humanoids. In *IEEE International Conference on Robotics and Automation (ICRA)*, Vol. 1, pp. 491–496, 2003.

[19] M. Plooij, G. Mathijssen, P. Cherelle, D. Lefeber, and B. Vanderborght. Lock your robot: A review of locking devices in robotics. *IEEE Robotics & Automation Magazine (RAM)*, Vol. 22, No. 1, pp. 106–117, March 2015.

[20] MIKI PULLEY. Electromagnetic tooth clutches. `http://www.mikipulley.co.jp/data/pdf/en/cb_ts_ct.pdf`. (last visited April 2018).

[21] Y. Kakiuchi, K. Kojima, E. Kuroiwa, S. Noda, M. Murooka, I. Kumagai, R. Ueda, F. Sugai, S. Nozawa, K. Okada, and M. Inaba. Development of humanoid robot system for disaster response through team nedo-jsk's approach to darpa robotics challenge finals. In *IEEE-RAS International Conference on Humanoid Robots (Humanoids)*, pp. 805–810, Nov 2015.

[22] M. Wisse, A. L. Schwab, and F. C. T. van der Helm. Passive dynamic walking model with upper body. *Robotica*, Vol. 22, No. 06, pp. 681–688, 2004.

[23] R. Featherstone. *Rigid Body Dynamics Algorithms*. Springer-Verlag New York, Inc., Secaucus, NJ, USA, 2007.

[24] M. Azad, V. Ortenzi, H. C. Lin, E. Rueckert, and M. Mistry. Model estimation and control of compliant contact normal force. In *IEEE-RAS 16th International Conference on Humanoid Robots (Humanoids)*, pp. 442–447, Nov 2016.

[25] S. Noda, Y. Kakiuchi, H. Takeda, K. Okada, and M. Inaba. Goal-oriented simulation-based motion interpolator for complex contact transition: Experiments on knee-contact behavior. In *IEEE-RAS International Conference on Humanoid Robots (Humanoids)*, Nov 2018.

[26] T. P. Runarsson and X. Yao. Stochastic ranking for constrained evolutionary optimization. *IEEE Transactions on Evolutionary Computation*, Vol. 4, No. 3, pp. 284–294, Sep 2000.

[27] S. G. Johnson. The nlopt nonlinear-optimization package. `http://ab-initio.mit.edu`.

[28] K. K. Yin, K. Loken, and M. van de Panne. Simbicon: Simple biped locomotion control. In *ACM Transactions on Graphics (TOG)*, Vol. 26, p. 105, 2007.

[29] K. N. K. Nguyen, S. Noda, Y. Kojio, F. Sugai, S. Nozawa, Y. Kakiuchi, K. Okada, and M. Inaba. Robust and stretched-knee biped walking using direct joint angle control. In *IEEE/RSJ International Conference on Intelligent Robots and Systems (IROS)*, pp. 1247–1254, Oct 2018.

[30] J. Tan, Z. Xie, B. Boots, and C. K. Liu. Simulation-based design of dynamic controllers for humanoid balancing. In *IEEE/RSJ International Conference on Intelligent Robots and Systems (IROS)*, pp. 2729–2736, Oct 2016.

[31] K. Ayusawa, G. Venture, and Y. Nakamura. Identifiability and identification of inertial parameters using the underactuated base-link dynamics for legged multibody systems. *The International Journal of Robotics Research (IJRR)*, Vol. 33, No. 3, pp. 446–468, 2014.

[32] S. O. H. Madgwick, A. J. L. Harrison, and R. Vaidyanathan. Estimation of imu and marg orientation using a gradient descent algorithm. In *IEEE International Conference on Rehabilitation Robotics*, pp. 1–7, June 2011.